Finetuning the Microstructure of Metal-Oxide Targets to Optimize Sputter Behavior for Thin Films in TFT

E. Franzke**, Z. Gao*, D. Zacharias**, H. Schmidt***
***Plansee Shanghai, China**
****Plansee SE, Reutte, Austria**
*****Plansee LLC, Franklin, MA, U.S.A**

Abstract

Films of Molybdenum- and Tungsten-Oxides are used as low reflection dark layers to cover thin metal line as well as high work-function materials. Due to their nature as sub stoichiometric oxides with composition tailored to specific applications, sputter targets used in the process compose of different material phases on the micrometer scale. We study the impact of microstructure on the sputter behavior.

Author Keywords

Sub stoichiometric oxides, dark layers, high work function materials, Raman spectroscopy

1. Introduction: Mo & W oxides and applications

Metal-Oxides targets have been long applied in the manufacturing process of high-end flat panel displays for example as transparent electrodes of ITO. Dark MoOx films on the other hand can be used to cover reflecting areas and provide increase contrast ratios under ambient conditions. This is exemplarily shown in figure 1 a, b for different film thicknesses. The underlying multibeam interference effect due to different refractive indices in the layers leads to reflection levels below 5%. By varying the oxygen content and second metal-doping in the target, the optical and electronic properties can be tuned. Other applications can be addressed by adding additional O2 during film deposition, MoOx or WOx films show interesting electronic properties as hole injection layers, work function measured by UPS are show in figure 1d. Values can be tuned from around 4.6ev to 5.2ev for films with a composition of close to MoO3. MoOx films are introduced as hetero stacks with TiOx as ITO replacement for perovskite solar cells.

Thin films for large scale TFT (thin film transistors) arrays are commonly deposited by PVD / sputter deposition. Being only a few 100-nanometer thick, film quality and the production scale control is essential for performance and scalability of these devices. To this end, the property of the sputter targets themselves play a crucial role in in the process. For example, microstructural in uniformity could lead to variation in sputter rates and therefore film thickness. Dielectric inclusions on the other hand could mitigate higher arcing behavior, increasing the defect rate.

2. Sputter target & microstructures

Sputter targets of high melting refractory metals and oxide material are usually produced using a powder metallurgical approach. For this, powders are refined, mixed and compacted and sintered. Techniques such as hot pressing (HP) and hot isostatic pressing (HIP) can produce targets with superior density and phase homogeneity. Thin film properties can be significantly influenced by the choice of sputtering target materials, especially

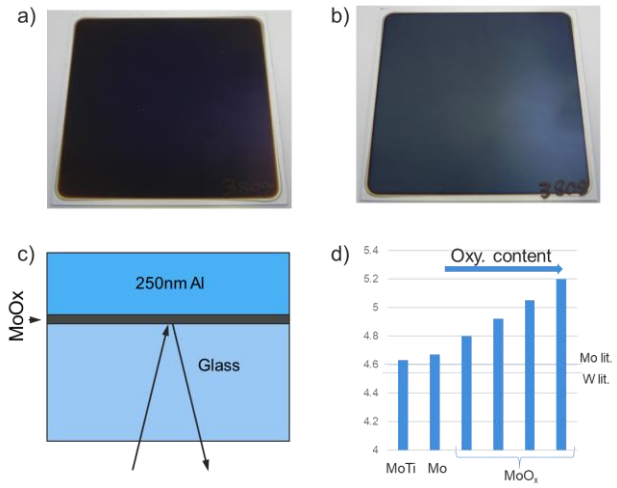

Figure 1.a) b) Metal Oxides of 50nm covering reflective metal films for dark appearance. C) Multibeam interference creates the black effect. D) work function of metal and metal oxide films measured by UPS. The films are tuned by oxygen content to finetune work function. Literature values are indicated by the lines

when advanced powder metallurgical techniques are employed. These techniques allow for precise control over the composition, purity, and microstructure of the target materials, which in turn affects the electrical, optical, and mechanical properties of the resulting thin films. The microstructure of the target material, including grain size and phase distribution, can influence the uniformity and adhesion of thin films. Additional alloying elements can be added and distributed uniformly during powder mixing process which influences the target and thin film properties in sputtering application significantly.

ISSN 0097-996X/25/5601-0026-$1.00 © 2025

Figure 2. shows different Metal-Oxide target materials, which inhibit a similar overall chemical composition, but yield a very different microstructure on a local scale due to different pre-material and fabrication methods. Via Raman mapping, the different elements and material phases are identified and shown. Depending on the material oxide phases which are conductive, and insulating can be found. The images in Fig 2 depict local variations while the material is uniform on a large scale. These differences in microstructure are studied regarding the sputtering behavior.

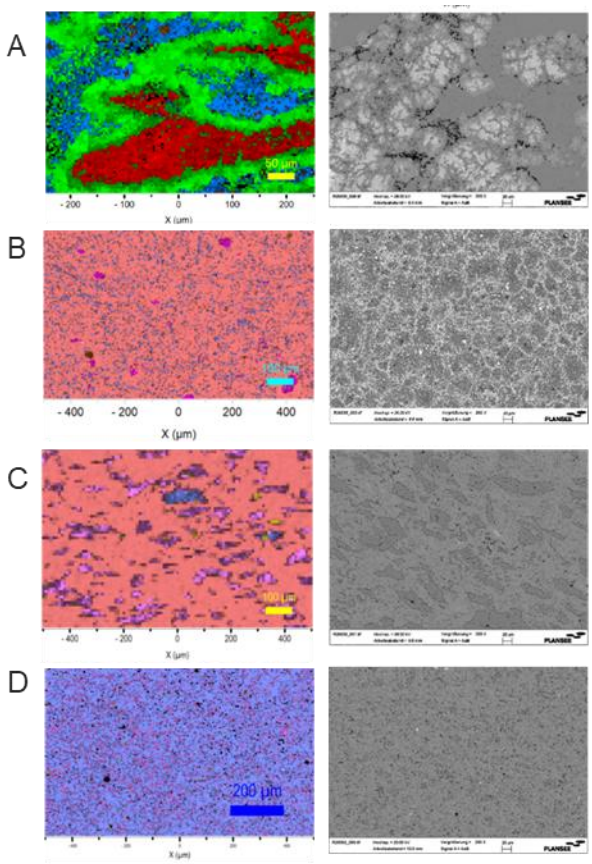

Figure 2. Exemplary microstructures and phase distributions based on Raman measurements (left) of target materials with the same chemical compositions. Different colors indicate different oxidation states, i.e. phases.

3. Physical vapor deposition of MoOx: Erosion and surface evolution over time

We comment on CTE, oxygen addition, sputter powers of oxide vs. metallic targets. The sputtering tests was based on a combined multipiece target of four MoOx materials (A, B, C, and D), by a DC magnetron sputtering deposition system (HuaSheng MC800). Prior to sputtering, the chamber was vacuumized to under 2×10^{-3} Pa, without heating. The sputtering process was conducted in a pure Ar gas environment, with gas flow rate of 345sccm, to get a chamber pressure of 0.5 Pa. The multipiece target was then DC-sputtered at a power density of approximately 2.5 W/cm^2, without additional heating. To reach a deep erosion curve, the sputtering time was 35 h in total. To examine the erosion state of the target, after every veil hour sputtering, the target was measured regarding surface morphology and roughness. During the experiment, the variations in target voltage and current were recorded in real time. The roughness and 3D morphology of the coatings were assessed using a handheld roughness tester and a confocal laser scanning microscope (Olympus OLS4100), respectively. The erosion depth after different sputtering durations were measured by a profiler (Mitutoyo, CV3200). All the error bars in this paper are from standard deviation. The sputtering experimental results are presented in the following figures.

As shown in Fig.3 on the right-hand side, all targets show erosion profiles of around 2.5 mm depth after 35 hours sputtering. This is around a half thickness of the total target. The erosion curve of the targes side is general deeper than the other, which may be due to the magnet field is stronger than the right side. The left images of Fig.3 present optical pictures of the target surface with obvious different conditions. Targets A, B, and C show long and deep crack propagation, while target D does not, although it presents the highest electrical resistivity among them. This different crack can be attributed to a) different mechanical strength of the targets and b) to different heat conduction due to different microstructures leading to heat pockets, heat rates and thermal stresses. Overall, the coefficient of thermal expansion of MoOx is in the order of ($5.0*10^{-6}$ 1/K) and therefore significant below that of pure metals. Target D also depicts a much rougher surface than the others. Both of A and D show particles after long sputtering.

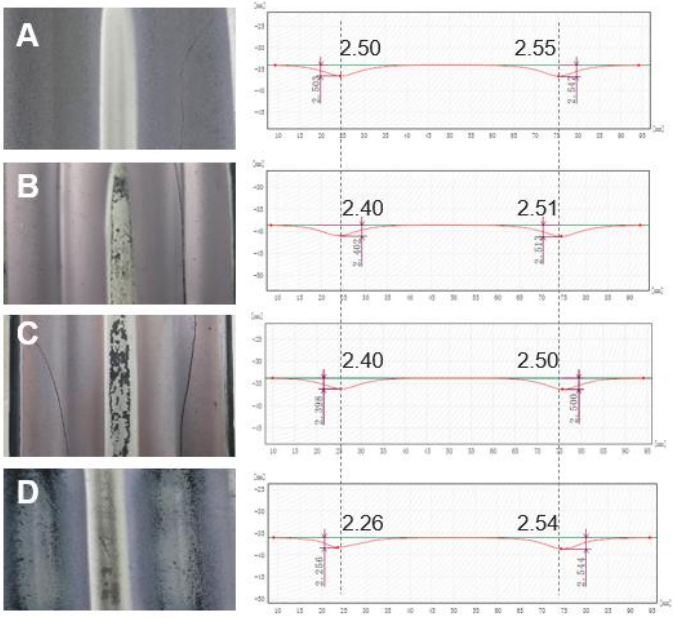

Fig. 3 Different target optical surface (left) and their erosion depth (right) records after 35 sputtering.

Fig. 4a shows the target voltage variation of the combined multipiece over 35 h sputtering. At a power density setting of 2.5 W/cm^2, the target voltage is decreasing with prolong sputtering

time, especially in the first 5 h. This means the target conductivity is getting better overall improved after sputtering. After 17 h sputtering, the target voltage remains stable. Some obvious voltage fluctuations happened because of unstable condition at a new round of sputtering test, which is after the target has been exposed to air surface tests. The erosion depth of sputtered targets after every 6 hours sputtering is shown in Fig. 4b. All the four materials depict similar erosion depth. The erosion rate of A is slightly higher than the others.

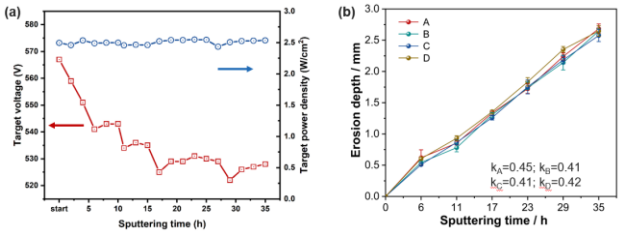

Fig. 4 (a) The targets voltage variation records during the whole sputtering process, (b) targets erosion depth records after every 6 hours sputtering.

To understand more about the evaluation of microstructure, at 3 points, after the 0h, 11h and 35h sputtering, the target 3D morphology is measured by a laser scanning microscope, as shown in Fig. 5. While already starting at different surface morphologies, these are evolving and increasing over time.

To study this more, the averaged surface roughness data is presented in Fig. 6a as a function of sputter time. Additionally, the targets roughness was also inspected by a handheld roughness tester after every 6 h sputtering, as shown in Fig. 6b.

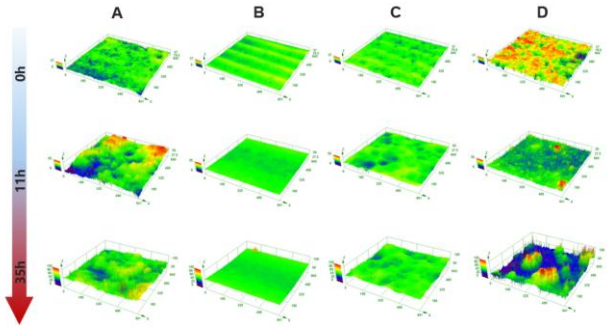

Fig. 5 The targets 3D surface morphology after a long-time sputtering, measured by a confocal laser scanning microscope.

Both analysis methods show the same findings:

1. Material B starts and remains a low roughness of 0.5 μm. As can be seen from the microstructure already, it consists of a very uniform and fine-grained material which shows beneficial properties in this regard.

2. The other examples are getting rougher and rougher during sputtering. It is also obvious that target D is the roughest target with a big error bar. Target A shows a comparable high roughness but slower getting roughness rate than target D. The surface evolution saturates over time for this example.

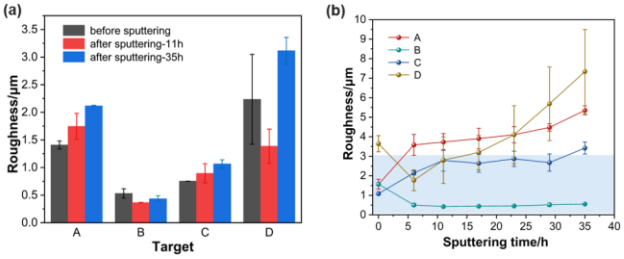

Fig. 6 The targets surface roughness after a long-time sputtering record (a) by a confocal laser scanning microscope, and (b) by a handheld roughness tester.

4. Conclusion

In our work, we show that the structure and phase composition of oxides materials can have a significant impact on overall surface roughness and more important on the evolution of the surface during sputtering. Depending on the material, this is known to have a profound impact on sputter properties like arcing, particles and redeposition and therefore on the resulting film properties as well as mass production and process stability. Knowing in detail which microstructure yield which behavior benefits process tuning and selection overall.

5. References

1. Y.X. Feng, S.M. Chen, A very dark-and-conductive electrode based on Mo/MoOx/ITO structure, Applied Surface Science 384 (2016) 348–352. http://dx.doi.org/10.1016/j.apsusc.2016.05.049

2. H. Köstenbauer, et al., "Molybdenum Oxides for Low-Reflectance Thin Films in Touch Applications", IDMC2013, paper PH-01 (2013).

3. H. Schmidt, et. al, "Sputtered Molybdenum-Oxide for Anti-Reflection Layers in Displays: Optical Properties and Thermal Stability", SID Digest 49, 225-229 (2018).

4. S. Wang, et al., "Lower Reflective TFT Materials and Technology Innovation," SID Digest 48, 1479-1481 (2017).

5. D. Lee, D. Kim, Y. Lee, D. Y. Jeon, Work function Engineering of Graphene Anode by Solution Processible MoOx-doping for Efficient Polymer Light-Emitting Diodes, SID Symposium Digest of Technical Papers, 48 (2017), P-232L http://dx.doi.org/10.1002/sdtp.12070.

6. H. Roh, J. Roh, H. Shin, H. Kim, C. Lee, Reduced Contact Resistance with MoOx Injection Layer for Thin Film Transistors Based on Organic Semiconductors with Deep HOMO Level, SID Symposium Digest of Technical Papers, 47 (2016), P-109, https://doi.org/10.1002/sdtp.10993

7. Xiaoxiang Zhang, Yongzhi Song, et.al, Low reflectivity Material Development for Border-less LCD Product, SID Symposium Digest of Technical Papers, 47 (2019), P-164, https://doi.org/10.1002/sdtp.13320